

Geophysical Research Letters



RESEARCH LETTER

10.1029/2019GL086663

Key Points:

- We measure and date individual isochronal radar internal reflection horizons across the Weddell Sea sector of the West Antarctic Ice Sheet
- Horizons dated to 1.9–3.2, 3.5–6.0, and 4.6–8.1 ka are widespread and linked to previous radar surveys of the Ross and Amundsen Sea sectors
- These form the basis for a wider database of ice sheet architecture for validating and calibrating ice sheet models of West Antarctica

Supporting Information:

- Supporting Information S1

Correspondence to:

D. W. Ashmore,
d.ashmore@liverpool.ac.uk

Citation:

Ashmore, D. W., Bingham, R. G., Ross, N., Siegert, M. J., Jordan, T. A., & Mair, D. W. F. (2020). Englacial architecture and age-depth constraints across the West Antarctic Ice Sheet. *Geophysical Research Letters*, 47, e2019GL086663. <https://doi.org/10.1029/2019GL086663>

Received 15 DEC 2019

Accepted 27 FEB 2020

Accepted article online 2 MAR 2020

Englacial Architecture and Age-Depth Constraints Across the West Antarctic Ice Sheet

David W. Ashmore¹ , Robert G. Bingham² , Neil Ross³ , Martin J. Siegert⁴ , Tom A. Jordan⁵ , and Douglas W. F. Mair¹

¹School of Environmental Sciences, University of Liverpool, Liverpool, UK, ²School of GeoSciences, University of Edinburgh, Edinburgh, UK, ³School of Geography, Politics and Sociology, Newcastle University, Newcastle upon Tyne, UK, ⁴Grantham Institute and Department of Earth Science and Engineering, Imperial College London, London, UK, ⁵British Antarctic Survey, Cambridge, UK

Abstract The englacial stratigraphic architecture of internal reflection horizons (IRHs) as imaged by ice-penetrating radar (IPR) across ice sheets reflects the cumulative effects of surface mass balance, basal melt, and ice flow. IRHs, considered isochrones, have typically been traced in interior, slow-flowing regions. Here, we identify three distinctive IRHs spanning the Institute and Möller catchments that cover 50% of West Antarctica's Weddell Sea Sector and are characterized by a complex system of ice stream tributaries. We place age constraints on IRHs through their intersections with previous geophysical surveys tied to Byrd Ice Core and by age-depth modeling. We further show where the oldest ice likely exists within the region and that Holocene ice-dynamic changes were limited to the catchment's lower reaches. The traced IRHs from this study have clear potential to nucleate a wider continental-scale IRH database for validating ice sheet models.

Plain Language Summary Ice-penetrating radar is widely used to measure the thickness of ice sheets, critical to assessments of global sea level rise potential. This technique also captures reflections from chemical contrasts within the ice sheet, caused by the atmospheric deposition of conductive impurities, known as “internal reflection horizons” (IRHs) that can be traced over large distances. As these deposits are laid down in distinct events, most IRHs are isochronous age tracers and contain valuable information on past ice sheet processes. In this paper we trace and place age constraints on stratigraphic horizons across a large portion of the West Antarctic Ice Sheet, including regions where fast ice flow has disrupted the ice sheet stratigraphy. The resulting data set allows us to identify where the oldest ice is buried in the study region and provides evidence that flow of the ice sheet interior has been stable during the Holocene. Our results can be used to test the performance of ice sheet models, which seek to simulate the response of ice sheets to long-term environmental change.

1. Introduction

Projecting the future of the West Antarctic Ice Sheet (WAIS) and its potential impacts on rising global sea level has developed into a major imperative over recent decades, in response to satellites observing pervasive ice loss (Shepherd et al., 2019) that may indicate the onset (Feldman & Leverman, 2015) of a predicted collapse (Mercer, 1978). However, in order to have confidence in the ice sheet models used to predict such behavior, they must be informed and calibrated by data-driven constraints on ice behavior preceding the observational era. To date, such constraints have primarily been provided by paleoclimatic information drawn from surface-exposure dating, marine sediments and geomorphology, and ice cores (RAISED Consortium, 2014; Steig & Neff, 2018). By contrast, few studies have taken advantage of a valuable paleoclimatic resource that exists across much of Antarctica, namely, the internal stratigraphic architecture of the ice itself that has been sounded across much of the continent by ice-penetrating radar (IPR).

IPR is the primary method by which ice thickness has been measured across Antarctica (e.g., Fretwell et al., 2013). However, most IPR surveys have also sounded numerous englacial internal reflection horizons (IRHs) throughout the ice column (e.g., Steinhage et al., 2001; Winter et al., 2017), and these, away from density-driven reflectivity contrasts in the near-surface (Kovacs et al., 1995), and the strained ice of the basal zone where anisotropic effects become important (Fujita et al., 2000; Wang et al., 2018), are widely attributed

© 2020. The Authors.

This is an open access article under the terms of the Creative Commons Attribution License, which permits use, distribution and reproduction in any medium, provided the original work is properly cited.

to conductivity variations associated with the atmospheric deposition of impurities at the surface (Bingham & Siegert, 2007; Holschuh et al., 2018; Miners et al., 2002). With the exception of basal ice and erosional surfaces (e.g., Arcone et al., 2012; Cavitte et al., 2016; Holschuh et al., 2018), continuous IRHs can be considered isochronal and hence reflect the advection of paleo-ice surfaces. Consequently, their imaged architecture represents a record of surface mass balance (SMB), basal melt, and ice flow and has the potential to constrain and inform ice sheet models (Hindmarsh et al., 2006; Leysinger Vieli et al., 2011). An archive of IRHs developed recently for the Greenland Ice Sheet from IPR data demonstrates how such data, tied to ice core chronologies, can be used to build spatially distributed age-depth profiles across a polar ice sheet (MacGregor et al., 2015). This resource provides key evidence that ice flow throughout Greenland decelerated during the Holocene (MacGregor et al., 2016). Given the uncertainty that remains regarding the future of the WAIS (Bamber et al., 2019), the development of a similar archive of internal architecture across the WAIS, ultimately tied to ice core chronologies, has been established as an internationally agreed objective (e.g., <https://www.scar.org/science/antarchitecture/home/>).

The Institute and Möller Ice Streams (IMIS) comprises 50% of the total area of the WAIS that discharges to the Weddell Sea via the Filchner-Ronne Ice Shelf. Although not currently identified as a region of major ice loss by satellite altimetry (Shepherd et al., 2019), several recent studies, in part using IPR-sounded IRHs, have posited that the region has hosted significant ice-dynamical changes since the Last Glacial Maximum and through the Holocene (Bingham et al., 2015; Hillenbrand et al., 2014; Kingslake et al., 2016; Siegert et al., 2013; Siegert et al., 2019; Winter et al., 2015). Under climate change in the latter half of the 21st century a reorganization of ocean currents could increase melting considerably in the Filchner-Ronne Ice Shelf cavity (Hellmer et al., 2012), leading to marine ice sheet instability as the bed upstream of the grounding lines dips steeply upglacier (Ross et al., 2012).

We successfully trace three IRHs extensively across IMIS, into the upper part of the Ross Sea Sector of WAIS, and link two of these surfaces to IRHs previously traced across the Amundsen Sea Sector. The geometry of these isochrones reflects the combined effects of ice sheet accumulation, basal melt, and ice flow. We find a broad north-to-south shallowing of IRHs across IMIS reflecting the modern-day SMB gradient and consider evidence for IRH modification due to ice flow and/or basal melting. Placing broad age constraints on the traced IRHs, we infer that postulated Holocene reorganization of ice flow in the Weddell Sea sector was limited inland and that the oldest ice in the catchment underlies the onset region of IMIS. We conclude that the approach applied in this paper comprises a practical and effective method for developing a distributed database of englacial architecture and age-depth control across the wider West Antarctic Ice Sheet.

2. Methodology

Our principal data set comprises >25,000 line kilometers of airborne IPR data acquired across IMIS (Figure 1) during the austral season 2010/2011 using the British Antarctic Survey (BAS) Polarimetric radar Airborne Science Instrument (PASIN). Bed echoes from this survey (hereafter the “IMAFI” survey) have been used to map IMIS' subglacial roughness (Rippin et al., 2014) and geomorphology (Rose et al., 2014, 2015), notably revealing a reverse-sloping bed leading into a deep upstream basin that renders IMIS vulnerable to marine ice sheet instability (Ross et al., 2012; Siegert et al., 2016). Englacial IRHs from the same data set have also been analyzed to reveal that major ice flow pathways have switched within IMIS region throughout the Holocene (Bingham et al., 2015; Kingslake et al., 2018; Siegert et al., 2013; Winter et al., 2015), yet none of these previous analyses of englacial layering has traced individual isochrones across the region.

The IMIS IPR survey is well set up to trace IRHs, or isochrones, in three respects. First, the high number of crossovers and series of parallel transects acquired in the nested grid (Figure 1) afford multiple opportunities for linking horizons across intersecting IPR lines. Second, the IMAFI survey included several long profiles extending across the ice divides to Pine Island Glacier and the Ross Sea Sector Ice Streams. These profiles enable IRHs traced through the IMIS IPR data to be linked to IRHs traced through neighboring surveys. Third, the PASIN data acquisition for IMIS operated in two modes: a deep-looking 150 MHz center-frequency, 12 MHz bandwidth chirp mode designed primarily to sound the bed and englacial layering to ice depths of up to 4 km, and a shallower-probing 0.1 μ s unmodulated pulse mode optimized for sounding englacial layering in the upper few 100 m but also found to be capable of sounding deeper (~2 km, see

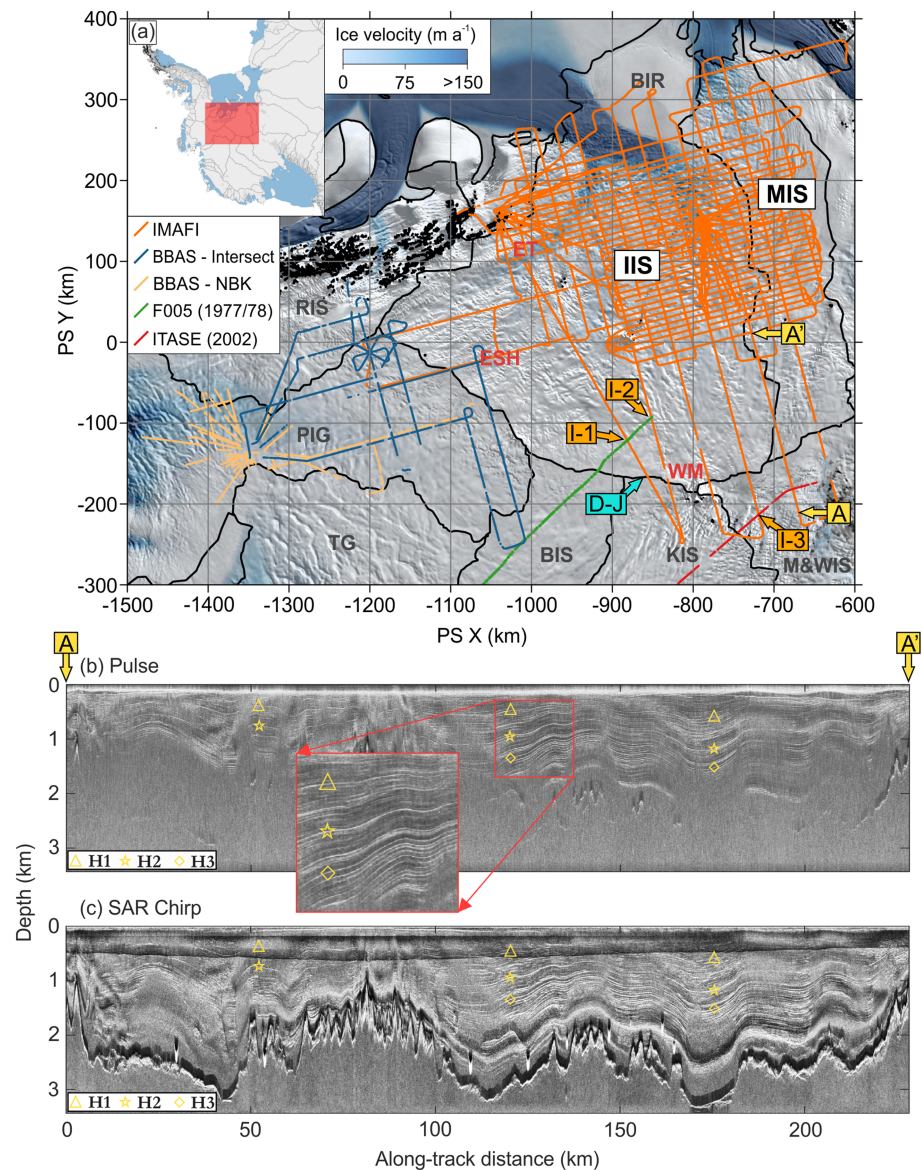


Figure 1. (a) The location of our study area (inset), its ice velocity (Mouginot et al., 2019), the data sets used in this study, our control line (A-A'), and major nearby ice catchment and subglacial features. The IPR data sets used in this study include 2010/2011 PASIN survey of IMIS (known as IMAFI); flights from the 2004/2005 PASIN survey of PIG (known as BBAS; Vaughan et al., 2006) which intersect IMAFI (BBAS – Intersect); 2004/2005 PASIN BBAS flightlines in which Karlsson et al. (2014) picked their “layer package” using chirp mode (BBAS – NBK); F005 from the 1977/1978 SPRI-NSF-TUD survey that intersects IMAFI at points I-1 and I-2; and the 2002 ITASE ground survey that intersects IMAFI at point I-3. D-J marks the site where we carry out our age-depth modeling. Ice catchment features: Bungenstock Ice Rise (BIR); Institute Ice Stream (IIS); Möller Ice Stream (MIS); Pine Island Glacier (PIG); Thwaites Glacier (TG); Bindschadler Ice Stream (BIS); Kamb Ice Stream (KIS); and Mercer and Whillans Ice Streams (M&WIS). Subglacial features: Ellsworth Trough (ET); Ellsworth Subglacial Highlands (ESH) and Whitmore Mountains (WM). Background image is MOA (Scambos et al., 2007). Map projection, and for figures herein, is EPSG: 3031. (b) The control line using the unmodulated pulse mode, H1–H3 marked with yellow symbols. (c) The control line using the chirp mode and SAR processing, H1–H3 marked with yellow symbols.

Figure 1b) in the ice. Fuller technical details of the PASIN data are provided by Jeffrey et al. (2018). In a preliminary analysis, we found that both synthetic-aperture radar (SAR)-focused chirp data and the “near-surface” pulse returns were capable of imaging consistent sets of englacial layering through the ice column across much of IMIS (Figure 1).

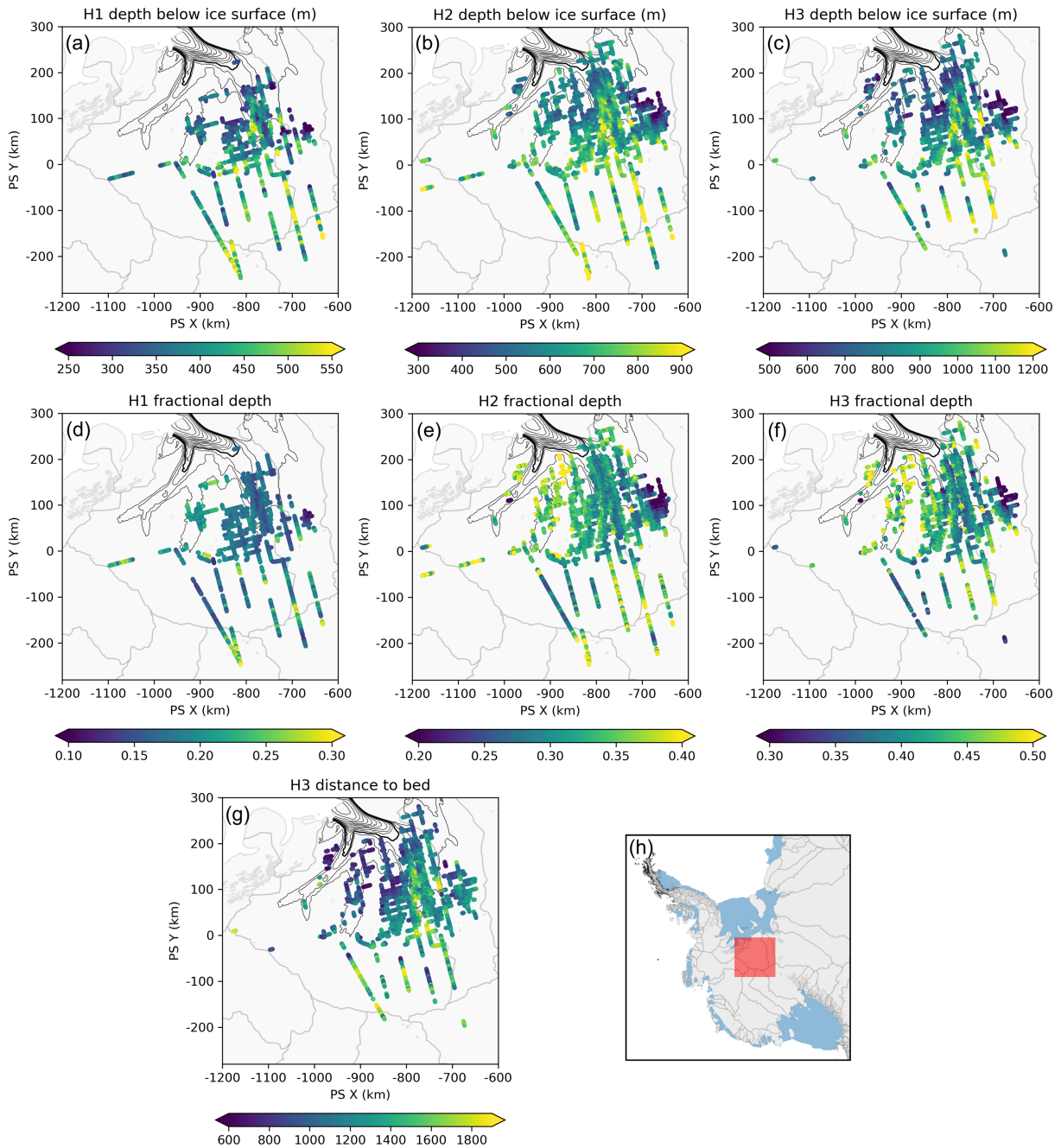


Figure 2. Results of the IRH tracking, showing (a–c) depth below surface, (d–f) fractional depth, and (g) the vertical thickness between the deepest IRH, H3, and the bed. Regional ice divides (gray) and 25 m a⁻¹ ice velocity contours (100 m a⁻¹ contour in heavy black) are shown for orientation. (h) Extent of panels (a) to (g).

Our workflow for tracing englacial architecture across IMIS proceeded as follows. The IPR data were first optimized for display by removing the air-to-ice two-way travel time and then applying a custom gain function and a 10-trace horizontal averaging. The data were then converted to the standard 2D SEG-Y format for importing into Schlumberger Petrel®, a 3D visualization and analysis software package designed for seismic data. To begin tracing IRHs, we identified a control IPR line running broadly along flow in the central IMIS catchment from the Weddell-Ross divide in which multiple IRHs are clearly visible (Figure 1). Within this line, and in complementary radargrams produced separately from the chirp and pulse data acquisition, we identified three control IRHs, H1–H3, from as wide a range of depths as possible (Figure 1). H1 and H2,

the shallower IRHs, are the brightest and most traceable IRHs along the control line, but below H2 it is less clear which IRH is most traceable. We elected to pick H3 on the basis that together with H2 it forms a recognizable IRH package analogous to that identified by Karlsson et al. (2014) within Pine Island Glacier. The H2/H3 IRH package bounds a distinct relatively low-reflectivity section of the ice column, with a grouping of closely spaced IRHs in its lower third which can often appear together as a diffuse group (Figure 1). A further diagnostic quality for H3 is that it forms the shallower of a bright couplet of IRHs.

Having traced IRHs H1–H3 along the control line, we progressively traced the same IRHs extending along IPR transects intersecting the control line, moving successively outward from the control line across the survey grid. Tracing typically ceased wherever these IRHs faded out due to steeply dipping reflector geometry or entering disrupted stratigraphy, such that no further clear connection could be made by navigating around intersecting lines or through comparisons with parallel lines. We note that in several areas of IMIS where we have not identified H1–H3, there are IRHs visible in the radargrams that might also be H1–H3, but we did not identify them with the diagnostic criteria outlined above. All resulting IRH picks were converted to depth below the ice surface using an electromagnetic wave speed of $168.5 \text{ m } \mu\text{s}^{-1}$ (Supporting Information Text S1) and a spatially invariant correction of +10 m to account for the near-surface high-velocity firn layer (Fujita et al., 2000; Dowdeswell & Evans, 2004; Kreuz et al., 2011; see Text S2). We attach a conservative uncertainty of $\pm 15 \text{ m}$ to our IRH depths arising from the firn correction, IPR system parameters, and variation in electromagnetic wave speed (see Text S3).

To place age constraints on our traced IRHs we examined their intersections with previously dated IRHs derived from earlier airborne and ground-based surveys (see Text S4). Four IRHs traced in a 1977/1978 flight of the Scott Polar Research Institute – National Science Foundation – Technical University of Denmark (SPRI-NSF-TUD) surveys (Siegert et al., 2005) intersect with the IMAFI survey in the upper catchment and are tied to the Byrd Ice Core chronology (Siegert & Payne, 2004). Their ages and stated uncertainties are $3.1 \pm 0.160 \text{ ka}$; $5.6 \pm 0.175 \text{ ka}$; $6.4 \pm 0.181 \text{ ka}$; $16 \pm 0.324 \text{ ka}$, arising from an IPR depth resolution of $\pm 40 \text{ m}$. Additionally, a deeper reflection in the ITASE traverse, intersecting the IMAFI survey in the upper Mercer/Whillans catchment (Figure 1), was dated to 17.5 ka at Byrd (Jacobel & Welch, 2005). Both the SPRI-NSF-TUD and ITASE data sets were acquired at lower frequency and therefore do not image at the same vertical resolution as the IMAFI survey. To provide an independent validation of these estimated IRH ages we apply a simple accumulation-driven one-dimensional age-depth model after Dansgaard and Johnsen (1969), this model having previously been applied to date IRHs (Fahnestock et al., 2001; Siegert & Payne, 2004; Karlsson et al., 2014). We choose a suitable location on an IMAFI survey line where this model is likely valid (Site D–J in Figure 1a), and a realistic range of values for ice accumulation as informed by contemporary (Arthern et al., 2006; van Wessem et al., 2018) and Holocene (Fudge et al., 2016; Koutnik et al., 2016) estimates, and for basal shear layer thickness (see Text S5). We examine the relationship between our IRHs and those identified in Pine Island Glacier (Text S6) by Karlsson et al. (2014) and the Internal-Layering Continuity Index (ILCI; Karlsson et al., 2012), a proxy for IRH preservation, after Bingham et al. (2015; Text S7).

3. Results

Figure 2 shows that H1, H2, and H3 were traceable widely across the IMIS catchments, traversing several of the ice stream tributaries as well as slow-flowing areas in between. Only in the downstream regions of fast flow (surface velocity $> 100 \text{ m a}^{-1}$; representing 4.3% of total IMIS catchment area) did IRH tracing prove impossible, although tracing was also precluded in some areas due to flow being disrupted by significant subglacial protuberances and subglacial mountain ranges (Figure 1). Some variation exists between each IRH in terms of the proportion of the survey tracks in which it is detectable. H1, H2, and H3 were traced in 16%, 31%, and 23% of the survey IPR tracks respectively, but in general, their traceability covers a similar areal distribution, with layering most detectable across the central IMIS region, effectively the onset region of both IIS and MIS (Figure 2). H1 and H2 were also traced along several IPR lines linking over the ice divide into the Mercer/Kamb Ice Stream catchments and H2 also extended into the Pine Island Glacier catchment. The deeper IRHs, H2 and H3, were more readily detectable than H1 nearer to the ice margin, being recoverable across the high ground grid north of Ellsworth Trough (Figure 1) Tributary and extending further than H1 into downstream MIS.

From H1 to H3 respectively, each traced IRH shows greater variability in depth below the ice surface and fraction of ice thickness (where 0/1 is the ice surface/bed). Text S1 and Table S1 provide fuller summary statistics for each IRH. IRHs are notably shallower toward the south of the region and generally the deepest in the ice column over the ice divides (Figure 2). From here, deeper IRHs track into the central IMIS onset zone, corresponding with a deep trough at the ice bed. In Figure 2g we show the distance of our deepest IRH, H3, to the ice bed, demonstrating that up to ~1,700 m of ice exists beneath it.

Figure 3 shows the relationship between our picked layers H1–H3 and the dated IRHs of Siegert and Payne (2004) at two intersections (I-1 and I-2); their relative depths are also provided in Table S2. At I-1, there is a marked correspondence between our IRHs and those of Siegert and Payne (2004), especially considering the unconstrained uncertainties associated with these pioneering surveys (see Text S4). Here (Figures 3a and 3b), H1 and their 3.1 ka layer are vertically offset by 18 m; and H2 and their 5.6 ka layer are offset by 14 m. This is good evidence that the different radar systems both detected the same dielectric contrasts in the ice. At I-2, close to the end of the SPRI-NSF-TUD radargram where there are high levels of clutter and saturation (see Siegert et al., 2005, their Figure 4a), H2 and their 5.6 ka layer are offset by 52 m (Figures 4c and 4d). For deeper IRHs, any correspondence between IRHs is less clear. Siegert and Payne's (2004) 6.4 ka layer broadly corresponds to our H3 (61 m offset at I-1) but lies within a thicker zone of bunched and diffuse reflectors (Figures 3a and 3b). It is not clear which IRHs in the IMIS survey correspond to Siegert and Payne's (2004) 16 ka layer, broadly occurring within a diffuse and smeared zone several hundred meters thick (Figure 3). Figures 3e and 3f show the crossover with the ITASE 2002 survey and the depth of the 17.5 ka layer (Jacobel & Welch, 2005). At I-3, we were only able to trace H1 (385 m depth) and not H2 nor H3 due to slope-induced fading of the returned IPR power at the point of crossover. At I-3, the 17.5 ka layer corresponds to a thick diffuse layer similar to Siegert and Payne's (2004) 16 ka layer (Figures S2f and S2g). This is likely the 17.5 ka IRH which manifests as a bright single reflection in the lower-frequency, lower-resolution ITASE survey.

Our age-depth modeling at Site D-J indicates ages for H1 as 1.9–3.2 ka; H2 as 3.5–6.0 ka; and H3 as 4.6–8.1 ka (Tables S3–S5), consistent with the ages as estimated by the association of the two sets of IRHs at I-1 (Figure 3a). Figures S1 and S2 and Text S1 provide strong evidence that Karlsson et al.'s (2014) “layer package” mapped across Pine Island Glacier is equivalent to the H2 and H3 in this study. Our H2 and H3 are therefore also widespread in the central Pine Island Glacier catchment. From the same workflow we hypothesize that the Siegert and Payne's (2004) 3.1 and 5.6 ka layers are our H1 and H2 and thus that these same layers must extend across Bindschadler Ice Stream and deep into Thwaites Glacier along the SPRI-NSF-TUD flight line.

4. Discussion

Our results demonstrate that, using IPR data acquired with appropriate parameters, englacial architecture can be traced reliably over wide swathes of dynamic ice through West Antarctica. Notably all previous studies exploiting PASIN data to analyze deep echoes (e.g., Bingham et al., 2015; Karlsson et al., 2014) have only used chirp mode. Here we have shown that the PASIN pulsed data acquisition captures englacial architecture at sufficient clarity to allow IRH tracing to ~2 km. This demonstrates a previously unknown utility of the PASIN archive, which covers large parts of West and East Antarctica, for IRH tracing. With reference to the ability to trace IRHs over dynamic ice, almost all previous englacial tracing in Antarctica performed to date has been along or around ice divides, where ice dynamics has not disrupted flow or introduced discontinuities (e.g., Cavitte et al., 2016; Siegert et al., 1998; Siegert et al., 2005; Siegert & Hodgkins, 2000; Winter et al., 2019). Siegert et al. (2005) were able to trace some IRHs across the Siple Coast Ice Streams from the 1970s SPRI-NSF-TUD surveys, but few were traceable across IMIS. Here we have revealed that IRHs (and ultimately paleo-surfaces) can be traced widely across the IMIS catchment, with IRHs reaching almost to the ice margin and IRHs traceable across all but the fastest-flow regions. The greatest challenge to IRH traceability in this region is imposed by ice flow across and/or around significant bedrock obstacles, which is likely to be more acute across IMIS, with its complex subglacial topography (Rippin et al., 2014; Ross et al., 2014) than for other WAIS catchments. The locations of the traceable IRHs correspond well with variations in the ILCI across IMIS derived by Bingham et al. (2015). ILCI is statistically higher where IRHs could be traced in this study (Figure S3 and Text S7). This is the first explicit demonstration of a direct correspondence between

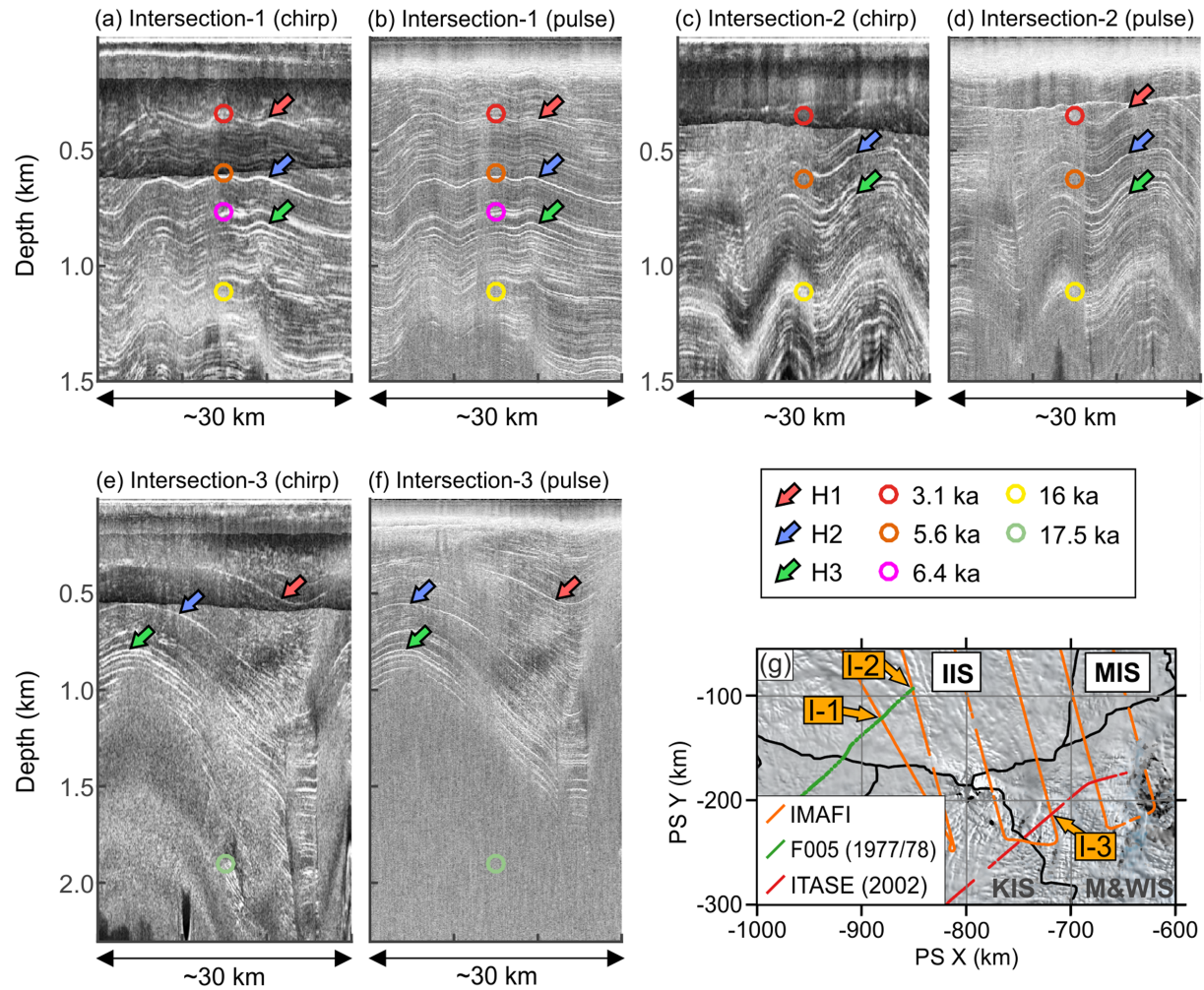


Figure 3. IMAFI radargrams and traced IRHs (arrows) at three intersections with published, dated traced IRHs (circles). (g) Locations of the three intersections (I-1, I-2, and I-3), abbreviations and associated references as in Figure 1.

ILCI and manual IRH traceability. This demonstrates that the wider application of ILCI across Antarctic IPR data sets can provide a robust indication of IRH traceability across the ice sheet.

IRH geometry is widely ascribed to the cumulative effect of SMB, ice dynamics, and basal melt (Leysinger Vieli et al., 2011). Mean modeled SMB from 1976 to 2016 (van Wessem et al., 2018) shows a modest increasing SMB gradient from the southern margins of IMIS (see Figure S4), close to the Transantarctic Mountains, to its northern margin and the divide with Pine Island Glacier. Assuming H1 and H2 are accurately dated at I-1, the validity of the local layer approximation (Waddington et al., 2007), and a steady state, we estimate the apparent mean (± 1 SD) accumulation across the catchment after MacGregor et al. (2016) since 5.6 ka to be 0.14 ± 0.026 m ice year⁻¹ (Text S8). Although our implementation of this model is less-constrained than MacGregor et al. (2016), these results and their comparison to regional climate model output provide evidence that the large scale IRH pattern is controlled by SMB (Figure S5). However, considerable spatial heterogeneity and high-frequency variation remain.

As one useful analogue to the possible processes occurring in our study area, Leysinger Vieli et al. (2007) employed an idealized flow-tube model to show the effects that areas of basal slip and basal melt can impose on 3D structure. They showed that IRHs will dip where basal motion transitions from low to high slip. We observe an increase (i.e., deepening) in fractional depth over the IIS tributary in the center of Figures 2d and 2f, which may be due to these effects. An alternative hypothesis for some IRH drawdown along transects that diverge from ice flowlines, such as those depicted in Figure 3, is glacial folding resulting from convergent

flow and ice anisotropy, such as that exemplified by Bons et al. (2016) at the onset of Greenland's Petermann Glacier. IMIS is known to have a complex flow history and packages of basal ice with distinct rheology (Bingham et al., 2015; Ross et al., 2019).

We also see some increase in fractional depth toward the ice divide (Figures 2e and 2f), which cannot be explained by the current flow field. In areas close to the ice divide, where ice flow is currently low, it is unlikely that variations in IRH depth are due to historical ice-dynamic changes as the existing evidence generally supports a stable Holocene WAIS divide (Ross et al., 2011). However, we note that close to South Pole (Beem et al., 2017; Bingham et al., 2007) and in regions of the WAIS (Siegert et al., 2004) some local reorganizations are thought to have occurred and left an imprint on IRH geometry. In the South Pole region such IRH draw-down proximal to an ice divide has been previously attributed to elevated geothermal heat flux (Jordan et al., 2018). Highly radiogenic Jurassic granites which could boost local geothermal heat flux by $\sim 30 \text{ mW m}^{-2}$, or 45% to 60% depending on the background heat flux, have been recognized in the Ellsworth Whitmore Mountains region (Leat et al., 2018). Basal melting close to the ice divide could provide an important source of water lubricating the flow of the ice further downstream.

We have placed broad constraints on three IRHs using intersections with previous surveys and age-depth modeling. It is imperative that future work can more directly link these distinctive IRHs with the ice core chronologies at WAIS Divide or Byrd using a modern airborne IPR system. The distance from the deepest, and oldest IRH we trace (H3), and the bed provides an indication of where the oldest ice within the IMIS catchment is. Considering the relative SMB distribution across the WAIS, this is perhaps some of the oldest ice in the WAIS. In the central catchment, for example, $\sim 1,700 \text{ m}$ of ice older than H3 ($\sim 6.4 \text{ ka}$) exists (Figure 2g). Close to the ice divide, $\sim 800 \text{ m}$ of ice exists below the 17.5 ka IRH (Jacobel & Welch, 2005; Figures 3e and 3f). Both the 17.5 and 16 ka (after Siegert & Payne, 2004) IRHs are broadly associated with a diffuse region of reflectivity several 100 m thick within IMIS (Ross et al., 2019). Tracing this diffuse zone would further elucidate where thick deposits of ice older than $\sim 17.5 \text{ ka}$ exist within IMIS. These dates, and the continuity of H3 to within 50 km of the grounding line, imply that the postulated Holocene retreat and readvance of WAIS (Kingslake et al., 2018; Siegert et al., 2013), and its mid-Holocene thinning (Hein, Marrero, et al., 2016), did not have a large effect on the inland portion of this part of the ice sheet. Similarly, the widespread occurrence of these IRHs suggests that the mid-Holocene flow reorganization of the IMIS region (Siegert et al., 2013) was confined to the catchment's lower regions. This supports IPR data suggesting a stable Holocene ice divide (Ross et al., 2011) and longer-term geochronological evidence which points to a relatively stable glaciological system at the WAIS divide over the last 1.4 Ma (Hein, Woodward, et al., 2016).

5. Conclusions

Through tracing IRHs along multiple flightlines over a $210,000 \text{ km}^2$ sector of the WAIS dissected by ice stream tributaries, we have demonstrated that tracing englacial IRHs, and ultimately englacial surfaces, is possible across the wider continental ice sheet. We traced three marker IRHs throughout the upper 50% of the ice column across IIS and MIS using previously underutilized pulsed PASIN IPR data acquired across the catchment in 2010/2011. We used intersections with previous data sets tied to Byrd Ice Core, central West Antarctica, and age-depth modeling to provide broad age constraints of 1.9–3.2 ka, 3.5–6.0 ka, and 4.6–8.1 ka for the IRHs. The IRH configurations across our study region imply that mid-Holocene flow reorganization of the IMIS region was spatially limited. The two lower layers that we traced are very likely the same layers identified by Karlsson et al. (2014) in Pine Island Glacier, providing a direct link to the Amundsen Sea Embayment, while our traced layers also connect into the Ross Sea sector of West Antarctica. By showing that IRHs can be traced across a catchment with a complex ice flow history and well away from ice divides, we have demonstrated encouraging prospects for tracing englacial surfaces extensively and reliably across Antarctica.

References

- Arcone, S. A., Jacobel, R., & Hamilton, G. (2012). Unconformable stratigraphy in East Antarctica: Part II. Englacial cosets and recrystallized layers. *Journal of Glaciology*, *58*(208), 253–264. <https://doi.org/10.3189/2012JG11J045>
- Arthern, R. J., Winebrenner, D. P., & Vaughan, D. G. (2006). Antarctic snow accumulation mapped using polarisation of 4.3-cm wavelength microwave emission. *Journal of Geophysical Research*, *111*, D06107. <https://doi.org/10.1029/2004JD005667>

Acknowledgments

D. W. A. would like to thank the Trans-Antarctic Association for Grant TAA-01-19 that allowed him to present and exchange ideas at the 2019 International Glaciological Society Radioglaciology Symposium. Thanks to the editor, Mattieu Morlighem, and Marie Cavitte and Joe MacGregor for their constructive and insightful comments. This paper was stimulated by the AntArchitecture Action Group of the Scientific Committee for Antarctic Research. Mapped IRHs are available online (<https://doi.org/10.5281/zenodo.3635940>). IMAFI IPR data were collected under NERC NE/G013071/1 and available from Siegert et al. (2017).

- Bamber, J. L., Oppenheimer, M., Kopp, R. E., Aspinall, W. P., & Cooke, R. M. (2019). Ice sheet contributions to future sea level rise from structured expert judgement. *Proceedings of the National Academy of Sciences*, *116*(23), 11,195–11,200. <https://doi.org/10.1073/pnas.1817205116>
- Beem, L. H., Cavitte, M. G. P., Blankenship, D. D., Carter, S. P., Young, D. A., Muldoon, G., et al. (2017). Ice-flow reorganization within the East Antarctic Ice Sheet deep interior. *Geological Society, London, Special Publications*, *461*, 35–47. <https://doi.org/10.1144/SP461.14>
- Bingham, R. G., Rippin, D. M., Karlsson, N. B., Corr, H. F. J., Ferraccioli, F., Jordan, T. A., et al. (2015). Ice-flow structure and ice dynamic changes in the Weddell Sea sector of West Antarctica from radar-imaged internal layering. *Journal of Geophysical Research: Earth Surface*, *120*, 655–670. <https://doi.org/10.1002/2014JF003291>
- Bingham, R. G., & Siegert, M. J. (2007). Radio-echo soundings over polar ice masses. *Journal of Environmental and Engineering Geophysics*, *12*(1), 47–62. <https://doi.org/10.2113/JEEG12.1.47>
- Bingham, R. G., Siegert, M. J., Young, D. A., & Blankenship, D. D. (2007). Organized flow from the South Pole to the Filchner-Ronne ice shelf: An assessment of balance velocities in interior East Antarctic using radio echo sounding data. *Journal of Geophysical Research*, *112*, F03S26. <https://doi.org/10.1029/2006JF000556>
- Bons, P. D., Jansen, D., Mundel, F., Bauer, C. C., Binder, T., Eisen, O., et al. (2016). Converging flow and anisotropy cause large-scale folding in Greenland's ice sheet. *Nature Communications*, *7*, 11427. <https://doi.org/10.1038/ncomms11427>
- Cavitte, M. G. P., Blankenship, D. D., Young, D. A., Schroeder, D. M., Parrenin, F., Le Meur, E., et al. (2016). Deep radio stratigraphy of the East Antarctic plateau: Connecting the Dome C and Vostok ice core sites. *Journal of Glaciology*, *62*, 323–334. <https://doi.org/10.1017/jog.2016.11>
- Dansgaard, W., & Johnsen, S. J. (1969). A flow model and a time scale for the ice core from Camp Century, Greenland. *Journal of Glaciology*, *8*(53), 215–223. <https://doi.org/10.3189/S0022143000031208>
- Dowdeswell, J. A., & Evans, S. (2004). Investigations of the form and flow of ice sheets and glaciers using radio-echo sounding. *Reports on Progress in Physics*, *67*(10), 1821–1861. <https://doi.org/10.1088/0034-4885/67/10/R03>
- Fahnestock, M., Abdalati, W., Joughin, I., Brozena, J., & Gogineni, P. (2001). High geothermal heat flow, basal melt, and the origin of rapid ice flow in central Greenland. *Science*, *294*(5550), 2238–2342. <https://doi.org/10.1126/science.1065370>
- Feldman, J., & Leverman, A. (2015). Collapse of the West Antarctic Ice Sheet after a local destabilization of the Amundsen Basin. *Proceedings of the National Academy of Sciences of the United States of America*, *112*, 14,191–14,196. <https://doi.org/10.1073/pnas.1512482112>
- Fretwell, P., Pritchard, H. D., Vaughan, D. G., Bamber, J. L., Barrand, N. E., Bell, R., et al. (2013). Bedmap2: Improved ice bed, surface and thickness data for Antarctica. *The Cryosphere*, *7*, 375–393. <https://doi.org/10.5194/tc-7-375-2013>
- Fudge, T. J., Markle, B. R., Cuffey, K., Buizert, C., Taylor, K. C., Steig, E. J., et al. (2016). Variable relationship between accumulation and temperature in West Antarctica for the past 31,000 year. *Geophysical Research Letters*, *43*, 3795–3803. <https://doi.org/10.1002/2016GL068356>
- Fujita, S., Matsuoka, T., Ishida, T., Matsuoka, K., & Mae, S. (2000). A summary of the complex dielectric permittivity of ice in the megahertz range and its applications for radar sounding of polar ice sheets. In T. Hondoh (Ed.), *Physics of ice core records* (pp. 185–212). Sapporo: Hokkaido University Press.
- Hein, A. S., Marrero, S. M., Woodward, J., Dunning, S. A., Winter, K., Westoby, M. J., et al. (2016). Mid-Holocene pulse of thinning in the Weddell Sea sector of the West Antarctic ice sheet. *Nature Communications*, *7*, 12511. <https://doi.org/10.1038/ncomms12511>
- Hein, A. S., Woodward, J., Marrero, S. M., Dunning, S., Steig, E. J., Freeman, S. P. H. T., et al. (2016). Evidence for the stability of the West Antarctic Ice Sheet divide for 1.4 million years. *Nature Communications*, *7*, 10325. <https://doi.org/10.1038/ncomms10325>
- Hellmer, H. H., Kauker, F., Timmermann, R., Determann, J., & Rae, J. (2012). Twenty-first-century warming of a large Antarctic ice-shelf cavity by a redirected coastal current. *Nature*, *485*(7397), 225–228. <https://doi.org/10.1038/nature11064>
- Hillenbrand, C.-D., Bentley, M. J., Stollard, T. D., Hein, A. S., Kuhn, G., Graham, A. G. C., et al. (2014). Reconstruction of changes in the Weddell Sea sector of the Antarctic Ice Sheet since the Last Glacial Maximum. *Quaternary Science Reviews*, *100*, 111–136. <https://doi.org/10.1016/j.quascirev.2013.07.020>
- Hindmarsh, R. C., Leysinger Vieli, G. J., Raymond, M. J., & Gudmundsson, G. H. (2006). Draping or overriding: The effect of horizontal stress gradients on internal layer architecture in ice sheets. *Journal of Geophysical Research*, *111*, F02018. <https://doi.org/10.1029/2005JF000309>
- Holschuh, N., Christianson, K., Conway, H., Jacobel, R. W., & Welch, B. C. (2018). Persistent tracers of historic ice flow in glacial stratigraphy near Kamb Ice Stream, West Antarctica. *The Cryosphere*, *12*, 2821–2829. <https://doi.org/10.5194/tc-12-2821-2018>
- Jacobel, R. W., & Welch, B. C. (2005). A time marker at 17.5 kyr BP detected throughout West Antarctica. *Annals of Glaciology*, *41*, 47–51. <https://doi.org/10.3189/172756405781813348>
- Jeofry, H., Ross, N., Corr, H. F. J., Li, J., Morlighem, M., Gogineni, P., & Siegert, M. J. (2018). A new bed elevation model for the Weddell Sea sector. *Earth System Science Data*, *10*, 711–725. <https://doi.org/10.5194/essd-10-711-2018>
- Jordan, T. A., Martin, C., Ferraccioli, F., Matsuoka, K., Corr, H., Forsberg, R., et al. (2018). Anomalously high geothermal flux near the South Pole. *Scientific Reports*, *8*(1), 16785. <https://doi.org/10.1038/s41598-018-35182-0>
- Karlsson, N. B., Bingham, R. G., Rippin, D. M., Hindmarsh, R. C. A., Corr, H. F. J., & Vaughan, D. G. (2014). Constraining past accumulation in the central Pine Island Glacier basin, West Antarctica, using radio-echo sounding. *Journal of Glaciology*, *60*, 553–562. <https://doi.org/10.3189/2014JoG13J180>
- Karlsson, N. B. K., Rippin, D. M., Bingham, R. G., & Vaughan, D. G. (2012). A 'continuity index' for assessing ice-sheet dynamics from radar-sounded internal layers. *Earth and Planetary Science Letters*, *335*–336, 88–94. <https://doi.org/10.1016/j.epsl.2012.04.034>
- Kingslake, J., Martin, C., Arthern, R. J., Corr, H. F. J., & King, D. C. (2016). Ice-flow reorganization in West Antarctica 2.5 kyr ago dated using radar-derived englacial flow velocities. *Geophysical Research Letters*, *43*, 9103–9112. <https://doi.org/10.1002/2016GL070278>
- Kingslake, J., Scherer, R. P., Albrecht, T., Coenen, J., Powell, D., Reese, R., et al. (2018). Extensive retreat and re-advance of the West Antarctic Ice Sheet during the Holocene. *Nature*, *558*(7710), 430–434. <https://doi.org/10.1038/s41586-018-0208-x>
- Koutnik, M. R., Fudge, T. J., Conway, H., Waddington, E. D., Neumann, T. A., Cuffey, K. M., et al. (2016). Holocene accumulation and ice flow near the West Antarctic Ice Sheet Divide ice core site. *Journal of Geophysical Research: Earth Surface*, *121*, 907–924. <https://doi.org/10.1002/2015JF003668>
- Kovacs, A., Gow, A., & Morey, R. M. (1995). The in-situ dielectric constant of polar revisited. *Cold Regions Science and Technology*, *23*, 245–256. [https://doi.org/10.1016/0165-232X\(94\)00016-Q](https://doi.org/10.1016/0165-232X(94)00016-Q)
- Kreutz, K., Koffman, B., Breton, D., & Hamilton, G. (2011). *Microparticle, conductivity, and density measurements from the WAIS divide deep ice core, Antarctica*. Boulder, CO: National Snow and Ice Data Center. <https://doi.org/10.7265/N5K07264>

- Leat, P. T., Jordan, T. A., Flowerdew, M. J., Riley, T. R., Ferraccioli, F., & Whitehouse, M. J. (2018). Jurassic high heat production granites associated with the Weddell Sea rift system, Antarctica. *Tectonophysics*, *722*, 249–264. <https://doi.org/10.1016/j.tecto.2017.11.011>
- Leyser Vieli, G. J.-M. C., Hindmarsh, R. C. A., & Siegert, M. J. (2007). Three-dimensional influences on radar layer stratigraphy. *Annals of Glaciology*, *46*, 22–28. <https://doi.org/10.3189/172756407782871729>
- Leyser Vieli, G. J.-M. C., Hindmarsh, R. C. A., Siegert, M. J., & Bo, S. (2011). Time-dependence of the spatial pattern of accumulation rate in East Antarctica deduced from isochronic radar layers using a 3-D numerical ice flow model. *Journal of Geophysical Research*, *116*, F02018. <https://doi.org/10.1029/2010JF001785>
- MacGregor, J. A., Colgan, W. T., Fahnestock, M. A., Mørlighem, M., Catania, G. A., Paden, J. D., & Gogineni, S. P. (2016). Holocene deceleration of the Greenland Ice Sheet. *Science*, *352*, 590–593. <https://doi.org/10.1126/science.aab1702>
- MacGregor, J. A., Fahnestock, M. A., Catania, G., Paden, J. D., Gogineni, S. P., Young, S. K., et al. (2015). Radiostratigraphy and age structure of the Greenland Ice Sheet. *Journal of Geophysical Research: Earth Surface*, *120*, 212–241. <https://doi.org/10.1002/2014JF003215>
- Mercer, J. H. (1978). West Antarctic Ice Sheet and CO₂ greenhouse effect: A threat of disaster. *Nature*, *271*, 321–325. <https://doi.org/10.1038/271321a0>
- Miners, W., Wolff, E., Moore, J., Jacobel, R., & Hempel, L. (2002). Modeling the radio echo reflections inside the ice sheet at Summit, Greenland. *Journal of Geophysical Research*, *107*(B8), 2172. <https://doi.org/10.1029/2001JB000535>
- Mouginot, J., Rignot, E., & Scheuchl, B. (2019). Continent-wide, interferometric SAR phase mapping, of Antarctic ice velocity. *Geophysical Research Letters*, *46*, 9710–9718. <https://doi.org/10.1029/2019GL083826>
- Steig, E. J., & Neff, P. D. (2018). The prescience of paleoclimatology and the future of the Antarctic Ice Sheet. *Nature Communications*, *9*(1), 2730. <https://doi.org/10.1038/s41467-018-05001-1>
- RAISED Consortium, Bentley, M. J., Cofaigh, C. O., Anderson, J. B., Conway, H., Davies, B., Graham, A. G., et al. (2014). A community based geological reconstruction of Antarctic Ice Sheet deglaciation since the Last Glacial Maximum. *Quaternary Science Reviews*, *100*, 1–9. <https://doi.org/10.1016/j.quascirev.2014.06.025>
- Rippin, D., Bingham, R., Jordan, T., Wright, A., Corr, H. F. J., Ferraccioli, F., et al. (2014). Basal roughness of the Institute and Möller Ice Streams, West Antarctica: Process determination and landscape interpretation. *Geomorphology*, *214*, 139–147. <https://doi.org/10.1016/j.geomorph.2014.01.021>
- Rose, K. C., Ross, N., Bingham, R. G., Corr, H. F. J., Ferraccioli, F., Jordan, T. A., et al. (2014). A temperate former West Antarctic Ice Sheet suggested by an extensive zone of subglacial meltwater channels. *Geology*, *42*(11), 971–974. <https://doi.org/10.1130/G35980.1>
- Rose, K. C., Ross, N., Jordan, T. A., Bingham, R. G., Corr, H. F. J., Ferraccioli, F., et al. (2015). Ancient pre-glacial erosion surfaces preserved beneath the West Antarctic Ice Sheet. *Earth Surface Dynamics*, *3*, 139–152. <https://doi.org/10.5194/esurf-3-139-2015>
- Ross, N., Bingham, R. G., Corr, H. F. J., Ferraccioli, F., Jordan, T. A., Le Brocq, A., et al. (2012). Steep reverse bed slope at the grounding line of the Weddell Sea sector in West Antarctica. *Nature Geoscience*, *5*, 393–396. <https://doi.org/10.1038/ngeo1468>
- Ross, N., Corr, H., & Siegert, M. (2019). Large-scale englacial folding and deep-ice stratigraphy within the West Antarctic Ice Sheet. *The Cryosphere Discuss*, in review. <https://doi.org/10.5194/tc-2019-245>
- Ross, N., Jordan, T. A., Bingham, R. G., Corr, H. F. J., Ferraccioli, F., Le Brocq, A., et al. (2014). The Ellsworth subglacial highlights: Inception and retreat of the West Antarctic Ice Sheet. *Geological Society of America Bulletin*, *126*, 3–15. <https://doi.org/10.1130/B30794.1>
- Ross, N., Siegert, M. J., Woodward, J., Smith, A. M., Corr, H. F. J., Bentley, M. J., et al. (2011). Holocene stability of the Amundsen-Weddell ice divide, West Antarctica. *Geology*, *39*(10), 935–938. <https://doi.org/10.1130/G31920.1>
- Scambos, T., Haran, T., Fahnestock, M., Painter, T., & Bohlander, J. (2007). MODIS-based Mosaic of Antarctica (MOA) data sets: Continent-wide surface morphology and snow grain size. *Remote Sensing of Environment*, *2-3*, 242–257. <https://doi.org/10.1016/j.rse.2006.12.020>
- Shepherd, A., Ivins, E., Rignot, E., Smith, B., van den Broeke, M., Veliconga, I., & The IMBIE team (2019). Mass balance of the Antarctic Ice Sheet from 1992 to 2017. *Nature*, *558*, 219–222. <https://doi.org/10.1038/s41586-018-0179-y>
- Siegert, M., Jeofry, H., Corr, H., Ross, N., Jordan, T., Ferraccioli, F., et al. (2017). *Synthetic-aperture radar (SAR) processed airborne radio-echo sounding data from the Institute and Möller ice streams, West Antarctica, 2010-11*. UK: Polar Data Centre, Natural Environment Research Council. <https://doi.org/10.5285/8a975b9e-f18c-4c51-9bdb-b00b82da52b8>
- Siegert, M., Ross, N., Corr, H., Kingslake, J., & Hindmarsh, R. (2013). Late Holocene ice-flow reconfiguration in the Weddell Sea sector of West Antarctica. *Quaternary Science Reviews*, *78*, 98–107. <https://doi.org/10.1016/j.quascirev.2013.08.003>
- Siegert, M. J., & Hodgkins, R. (2000). A stratigraphic link across 1100 km of the Antarctic Ice Sheet between the Vostok ice core site and Titan Dome (near South Pole). *Geophysical Research Letters*, *27*, 2133–2136. <https://doi.org/10.1029/2000GL008479>
- Siegert, M. J., Hodgkins, R., & Dowdeswell, J. A. (1998). A chronology for the Dome C deep ice-core site through radio-echo layer correlation with the Vostok ice core. *Geophysical Research Letters*, *25*, 1019–1022. <https://doi.org/10.1029/98GL00718>
- Siegert, M. J., Kingslake, J., Ross, N., Whitehouse, P. L., Woodward, J., Jamieson, S. S. R., et al. (2019). Major ice sheet change in the Weddell Sea Sector of West Antarctic over the last 5000 years. *Reviews of Geophysics*, *57*, 1197–1223. <https://doi.org/10.1029/2019RG000651>
- Siegert, M. J., & Payne, A. J. (2004). Past rates of accumulation in central West Antarctica. *Geophysical Research Letters*, *31*, L12403. <https://doi.org/10.1029/2004GL020290>
- Siegert, M. J., Pokar, M., Dowdeswell, J. A., & Benham, T. (2005). Radio-echo layering in West Antarctica: A spreadsheet database. *Earth Surface Processes and Landforms*, *30*, 1583–1591. <https://doi.org/10.1002/esp.1238>
- Siegert, M. J., Ross, N., Li, J., Schroeder, D. M., Rippin, D., Ashmore, D., et al. (2016). Subglacial controls on the flow of the Institute Ice Stream, West Antarctica. *Annals of Glaciology*, *57*, 19–24. <https://doi.org/10.1017/aog.2016.17>
- Siegert, M. J., Welch, B., Morse, D., Vieli, A., Blankenship, D. D., Joughin, I., et al. (2004). Ice flow direction change in interior West Antarctic. *Science*, *305*, 1948–1951. <https://doi.org/10.1126/science.1101072>
- Steinhage, D., Nixdorf, U., Meyer, U., & Miller, H. (2001). Subglacial topography and internal structure of central and western Dronning Maud Land, Antarctica, determined from airborne radio echo sounding. *Journal of Applied Geophysics*, *47*(3-4), 183–189. [https://doi.org/10.1016/S0926-9851\(01\)00063-5](https://doi.org/10.1016/S0926-9851(01)00063-5)
- Vaughan, D. G., Corr, H. F. J., Ferraccioli, F., Frearson, N., O'Hare, A., Mach, D., et al. (2006). New boundary conditions for the West Antarctic Ice Sheet: Subglacial topography beneath Pine Island Glacier. *Geophysical Research Letters*, *33*, L09501. <https://doi.org/10.1029/2005GL025588>
- Waddington, E. D., Neumann, T. A., Koutnik, M. R., Marshall, H.-P., & Moore, D. L. (2007). Inference of accumulation-rate patterns from deep layers in glaciers and ice sheets. *Journal of Glaciology*, *53*(183), 694–712. <https://doi.org/10.3189/002214307784409351>

- Wang, B., Sun, B., Ferrocchioli, F., Martin, C., Steinhage, D., Cui, X., & Siegert, M. J. (2018). Summit of the East Antarctic Ice Sheet underlain by extensive thick ice-crystal fabric layers formed by glacial-interglacial environmental change. *Geological Society, London, Special Publications*, *461*, 131–144. [https://doi.org/10.1144/SP461.1\(2018\)](https://doi.org/10.1144/SP461.1(2018))
- van Wessem, J. M., van de Berg, W., Noël, B. P. Y., van Meijgaard, E., Amory, C., Birnbaum, G., et al. (2018). Modelling the climate and surface mass balance of polar ice sheets using RACMO2 – Part 2: Antarctica (1979–2016). *The Cryosphere*, *12*, 1479–1498. <https://doi.org/10.5194/tc-12-1479-2018>
- Winter, A., Steinhage, D., Arnold, E. J., Blankenship, D. D., Cavitte, M. G. P., Corr, H. F. J., et al. (2017). Comparison of measurements from different radio-echo sounding systems and synchronisation with the ice core at Dome C, Antarctica. *The Cryosphere*, *11*, 653–668. <https://doi.org/10.5194/tc-11-653-2017>
- Winter, A., Steinhage, D., Creyts, T. T., Kleiner, T., & Eisen, O. (2019). Age stratigraphy in the East Antarctic Ice Sheet inferred from radio-echo sounding horizons. *Earth System Science Data*, *11*, 1069–1081. <https://doi.org/10.5194/essd-11-1069-2019>
- Winter, K., Woodward, J., Ross, N., Dunning, S. A., Bingham, R. G., Corr, H. F. J., & Siegert, M. (2015). Airborne radar evidence for tributary flow switching in Institute Ice Stream, West Antarctica: Implications for ice sheet configuration and dynamics. *Journal of Geophysical Research: Earth Surface*, *120*, 1611–1625. <https://doi.org/10.1002/2015JF003518>